# Femtosecond Spectroscopy of Au Hot-Electron Injection into TiO₂: Evidence for Au/TiO₂ Plasmon Photocatalysis by Bactericidal Au Ions and Related Phenomena

**Marina Radzig [1], Olga Koksharova [1,2] , Inessa Khmel [1] , Vladimir Ivanov [3], Khursand Yorov [2,3] , John Kiwi [4], Sami Rtimi [4] , Elina Tastekova [5], Arseny Aybush [5] and Victor Nadtochenko [2,5,*]**

[1] Institute of Molecular Genetics, Russian Academy of Sciences, Kurchatov Sq. 2, 123182 Moscow, Russia; radzig@yandex.ru (M.R.); koksharova@genebee.msu.su (O.K.); khmel@img.ras.ru (I.K.)

[2] A. N. Belozersky Institute of Physico Chemical Biology and Chemical Department of Lomonosov Moscow State University, 119992 Moscow, Russia; khursandy@gmail.com

[3] Kurnakov Institute of General and Inorganic Chemistry of the Russian Academy of Sciences, Leninskiy Av 31, 119991 Moscow, Russia; van@igic.ras.ru

[4] Ecole Polytechnique Fédérale de Lausanne, EPFL-SB-ISIC-GPAO, Station 6, CH-1015 Lausanne, Switzerland; john.kiwi@epfl.ch (J.K.); sami.rtimi@epfl.ch (S.R.)

[5] N. N. Semenov Institute of Chemical Physics, Russian Academy of Sciences, Kosigin str. 4, 119991 Moscow, Russia; e.tastekova@fmlab.ru (E.T.); arseny.aybush@chph.ras.ru (A.A.)

**\*** Correspondence: nadtochenko@gmail.com; Tel./Fax: +7-499-137-6676

check for updates

**Abstract:** In the present work, we provide evidence for visible light irradiation of the Au/TiO₂ nanoparticles' surface plasmon resonance band (SPR) leading to electron injection from the Au nanoparticles to the conduction band of TiO₂. The Au/TiO₂ SPR band is shown to greatly enhance the light absorption of TiO₂ in the visible region. Evidence is presented for the light absorption by the Au/TiO₂ plasmon bands leading to the dissolution of Au nanoparticles. This dissolution occurs concomitantly with the injection of the hot electrons generated by the Au plasmon into the conduction band of TiO₂. The electron injection from the Au nanoparticles into TiO₂ was followed by femtosecond spectroscopy. The formation of Au ions was further confirmed by the spectral shift of the transient absorption spectra of Au/TiO₂. The spectral changes of the SPR band of Au/TiO₂ nanoparticles induced by visible light were detected by spectrophotometer, and the morphological transformation of Au/TiO₂ was revealed by electron microscopy techniques as well. Subsequently, the fate of the Au ions was sorted out during the growth and biofilm formation for some selected Gram-negative bacteria. This study compares the bactericidal mechanism of Au ions and Ag ions, which were found to be substantially different depending on the selected cell used as a probe.

**Keywords:** plasmon photocatalysis; electron injection; gold nanoparticles; antibacterial effects; biofilms; DNA repair; genes expression; quorum sensing; porins

## 1. Introduction

TiO₂ photocatalysis induced by UV light possess powerful antimicrobial properties against bacteria, including multiresistant bacterial strains, viruses, and fungi. TiO₂ photocatalysts need UV-light photons with energies ≥3.2 eV. The photogenerated electron–hole pairs lead to the generation of reactive oxygen species (ROS) in aqueous solution, leading to the degradation of contaminants and

microorganisms [1,2]. Photocatalytic systems with biocidal effects under visible light are have not been widely reported and their mechanism of bacterial inactivation is only partially understood [3]. The photocatalytic/biocidal activity of Au/TiO$_2$ nanocomposites is higher compared to bare TiO$_2$ when excited by UV light. Electrons and holes are generated in TiO$_2$ due to the interband transition induced by the UV quanta absorption. Au promotes the electron/hole separation and leads to ROS formation [4,5].

Controversial results about the cytotoxicity of gold nanoparticles (Au-NPs) have been reported [6–8]. Antibacterial activity of Au nanoparticles against several bacteria has been suggested for *E. coli* and the *Bacillus* Calmette–Guérin antituberculosis strain of attenuated live bovine tuberculosis *Bacillus* (*Mycobacterium bovis* BCG) [8,9], and *Staphylococcus aureus* [10,11]. It has also been reported that spherical Au nanoparticles with a variety of surface modifiers were not inherently toxic to cells under dark conditions [11,12]. Some chemicals used as precursors of the Au nanoparticles have been reported to induce toxicity. In this case, the Au-NPs themselves did not lead to bacterial inactivation [11].

Uncoated Au-NPs present a low antibacterial activity under visible light due to surface plasmon resonance (SPR). Under low light intensity, the Au-NPs' heating was negligible [13]. Activity of Au-NPs becomes higher under light-emitting diode (LED) light providing a higher intensity radiation [14]. In parallel to the ROS production, Au nanoparticles activated by light may induce a photothermal bacterial inactivation as an additional effect [15–18].

The excitation of localized surface plasmons in Au-NPs generates hot electrons that transfer to the TiO$_2$ conduction band and significantly enhance the light-harvesting capabilities of the photocatalytic system [19,20]. The Au ions, as well as ions of other heavy metals, have been reported to lead to bacterial inactivation [21,22]. The mechanism of antibacterial action of Au ions on bacterial cells have scarcely been studied. The antibacterial activity of Au ions began to be used in medicine after the discovery of Robert Koch showing that gold cyanide presented bacteriostatic effects on tuberculosis pathogens. Au complexes have been investigated for the treatment of rheumatoid arthritis and cancer (more specifically, cytotoxic effect against melanoma and leukemia cells) [22–25]. The goal of the present work is to study the photocatalytic bactericidal effect under visible light due to the Au/TiO$_2$ nanoparticles' surface plasmon resonance band (SPR). This effect leads to electron injection from the Au nanoparticles to the conduction band of TiO$_2$, leading to the generation of Au ions. The antimicrobial effect of Au/TiO$_2$ nanoparticles induced by visible light was observed to be significant. This work investigates the effect of Au ions on the growth and biofilm formation of some Gram-negative bacteria. The data obtained in the present work indicate significant differences in the mode of interaction of Au ions compared to Ag ions on bacterial cells [26].

## 2. Materials and Methods

### 2.1. Preparation of Au/TiO$_2$ and Au Nanoparticles

The deposition of Au nanoparticles on TiO$_2$ (10 g/L) was carried out by photocatalytic reduction of Au$^{3+}$ ions in aqueous solution of HAuCl$_4$ (1 mM, Sigma-Aldrich Chemie GmbH, Steinheim, Germany). Methanol was added to the solution (8% volume) as a hole scavenger [19]. The suspension was irradiated for 20 min by an ultraviolet fluorescent lamp (wavelength 365 nm, intensity 50 mW/cm$^2$, Philips, Amsterdam, Dutch) under stirring. The Au/TiO$_2$ nanoparticles were washed away from the synthesis products for further experiments. The suspension was transferred to an Eppendorf tube and centrifuged for 15 min at 7000 rpm until complete precipitation of the particles. The solution above the precipitate was separated and the precipitate of Au/TiO$_2$ nanoparticles washed 15 times.

Au nanorods were synthesized according to the protocol reported by [27]. The details of the synthesis are presented in the Supplementary Information (Section SI1). The suspension of Au-NPs was centrifuged for 15 min at a speed of 7000 rpm until the precipitation of the particles was completed. The supernatant solution above the precipitate was separated and the precipitate washed for 15 times. The Au nanoparticles were suspended in a solution of PEG4000 (0.1 g/mL Merck

KGaA, Darmstadt, Germany). A scanning electron microscope (SEM) image of the Au nanoparticles is presented in Figure SI1.

The standard method of spherical Au-NP synthesis was used with some modifications [28]. The reduction of a $HAuCl_4$ solution was initiated by sodium tris-citrate (Sigma-Aldrich Chemie GmbH, Steinheim, Germany) and the solution was heated to the boiling temperature under stirring (SI1). When the solution (147 µL of 0.2 M $HAuCl_4$ in 100 mL water) reached 95 °C, the citrate solution (3 mL, 0.034 M) was added. After 20 min, the liquid was extracted and cooled to room temperature. A SEM image of the Au nanoparticles is present in Figure SI2.

## 2.2. Irradiation Procedures on the Au/TiO$_2$, Electron Microscopy, and Laser Femtosecond Experimental Setup

The photocatalytic effect of the $Au/TiO_2$ nanoparticles due to surface plasmon resonance (SPR) excitation was studied under the light of a light-emitting diode (LED, wavelength 530 nm, intensity 30 mW/cm$^2$, Nichia, Tokushima, Japan). The bacterial inactivation runs of the bacterial cells were run in an $Au/TiO_2$ suspension under a tungsten–halogen lamp: J118 500W R7s Phoenix (Linyi Yuhang Lighting Electric Appliance Co, Ltd, Shandong, China). The tungsten–halogen lamp spectrum is shown in the Supplementary Information Section SI2, Figure SI3). A cutoff infrared water filter (20 cm length, homemade) was used. The UV component of the light was blocked by a colored glass filter with a cutoff at 440 nm. The intensity of light reaching the sample was 60 mW/cm$^2$.

### 2.2.1. Electron Microscopy

The SEM images of Au-NPs and $Au/TiO_2$ nanoparticles were obtained with: (1) a Zeiss G25-SUPRA 25en01 (Carl Zeiss AG, Jena, Germany); (2) Carl Zeiss NVision 40, equipped with an Oxford X-Max X-ray detector. A voltage of 1 kV was used. The magnification of the micrographs ranged from 3000× to 300,000×. X-ray microanalysis was carried out at an accelerating voltage of 20 kV. Transmission electron microscope was a LEO 912 AB Omega (Carl Zeiss AG, Jena, Germany) with LaB6 cathode at a voltage of 100 kV.

### 2.2.2. Femtosecond Laser Photolysis Setup

A femtosecond pump (Spectra-Physics, Santa Clara, CA, USA)—supercontinuum probe setup was used to register the transient absorption (TA) spectra of the $Au/TiO_2$ colloids as reported recently [29]. The femtosecond pump pulse of 25 fs centered at 740 nm (1.68 eV) and a low fluency of 24 µJ/cm$^2$ was used to excite the $Au/TiO_2$ nanoparticles in solution. The pump and probe light spots had the diameters of 300 and 120 µm, respectively. The measured TA spectra were corrected for group delay dispersion of the supercontinuum using a protocol described previously [29]. Details of the femtosecond setup are shown in the Supplementary Information, Section SI3.

## 2.3. Preparation of Bacterial Strains, Evaluation of the Bacterial Inactivation Kinetics, and Bacterial Growth Conditions

Minimum inhibitory concentration (MIC) values for different strains of Gram-negative bacteria are shown in Table 1. Strains were maintained on Luria–Bertani broth solid agar (1.5% agar, LA, Sigma-Aldrich Chemie GmbH, Steinheim, Germany) at 30 °C. Difco Nutrient Broth (NB) and Difco Nutrient Agar (NA) were used in experiments with $AuHCl_4$. Antibiotics were added to the medium in the following concentrations (µg/mL): ampicillin (Ap, OAO "Biochemist", Moscow, Russia), 100; kanamycin (Km, OAO "Synthesis", Moscow, Russia), 100; tetracycline (Tc, Sigma-Aldrich Chemie GmbH, Steinheim, Germany), 20–40, gentamicin (Gm, KRKA, Novo mesto, Slovenia), 40; and rifampicin (Rif, Sigma), 50. The chemicals used during this study: $HAuCl_4 \cdot p$ $3H_2O$ (99.9%), $NaBH_4$ (99%), ascorbic acid (99%), cetyl-trimethyl-ammonium bromide (CTAB, 99%), trisodium citrate dihydrate, $AgNO_3$ (99%), and poly(ethylene glycol) PEG 40,000, were used as purchased (Sigma-Aldrich). $TiO_2$ Aeroxide® P25 (Degussa P25, Frankfurt, Germany) was used as received.

**Table 1.** Values for different strains of Gram-negative bacteria.

| Strains | MIC of AuHCl$_4$ (µg/mL)* |
|---|---|
| *Escherichia coli* AB1157 | $1.0 \pm 0.3$ |
| *Pseudomonas aeruginosa* PAO1 | $80 \pm 10$ |
| *Serratia proteamaculans* 94 | $1.4 \pm 0.3$ |

* The MIC values are a result of the data collected from 4 independent runs.

### 2.3.1. Minimum Inhibitory Concentrations (MICs) and Biofilm Formation

The MICs of AuHCl$_4$ were measured by serial twofold dilution [26]. The initial bacterial solution colony-forming units CFU/ml was ~$1 \times 10^5$ in nutrient broth (NB). The concentration of planktonic cells was evaluated by optical density at 600 nm (OD$_{600}$). The measurements were made after the incubation of bacteria for 24 h at 30 °C.

### 2.3.2. Biofilm Formation

The monitoring of the film formation was carried out following the protocol described by Zaitseva et al. [30]. Cells from fresh LA medium were inoculated into NB and incubated under shaking for 24 h at 30 °C. The culture was then diluted 300-fold in fresh NB, adding selected AuHCl$_4$ concentrations. Inoculated cultures were grown in 96-well polystyrene microtiter plates (150 µL per well) for 24 h at 30 °C under gentle shaking (105 rpm) to prevent the formation of sediment at the bottom of the wells. The growth of planktonic (unattached) cells was evaluated by measuring the optical density at 600 nm (OD$_{600}$) of the cell suspension. Biofilm formation was measured by discarding the medium, rinsing the wells with distilled water, and staining the attached cells with 1% w/v crystal violet (Reachim, Moscow, Russia). After staining for 45 min at 24 °C, the supernatant was then removed from the flask and the wells were rinsed three times with distilled water. Then, the biofilm-associated crystal violet was solubilized with ethanol and the absorbance measured at 600 nm. A microplate reader (Model 2550 Microplate Reader, Bio-Rad, Hercules, CA, USA) was used for measuring planktonic growth and biofilms. The mean CFU/ml for negative untreated samples were: ~$1.8 \times 10^8$; $2.2 \times 10^8$; $3.0 \times 10^8$ for *E. coli* AB1157, *P. aeruginosa* PAO1, and *S. proteamaculans* 94, respectively.

A bacterial growth time of 24 h was found to be optimal for biofilm formation. Experiments were repeated four times and bacteria were grown in eight replicate wells during each experiment. A study of cultures from wells under a microscope revealed no cell aggregates. The cell suspensions were turbid, which precludes the formation of aggregates. No biofilms were observed on the surface of the wells. Biofilms were formed on the well walls at the border of the medium surface and the air and not at the bottom of the wells.

### 2.3.3. Effect of AuHCl$_4$ on the *E. coli* AB1157 Biofilm and Effect of Au Ions on Bacterial Survival

An overnight culture of *E. coli* AB1157 was diluted 300-fold in NB, and thereafter the cells were grown on glass slides for 24 h at 30 °C, leading to the formation of biofilms. Then, the supernatant excess solution was removed from the slides and a fresh NB solution was added and supplemented with AuHCl$_4$. The bacterial cells were further grown for 24 h. Biofilms were analyzed by using crystal violet as described above. Bacterial viability in biofilms was assessed with Live/Dead BacLight Bacterial Viability and Counting Kit (Invitrogen, Molecular Probes) via scanning confocal laser microscopy (Zeiss LSM 510 laser module, Carl Zeiss GmbH, Jena, Germany) with an excitation wavelength at 488 nm.

### 2.3.4. Effect of Au Ions on *E. coli* AB1157 Cell Survival in Stationary and Exponential Growth Phases

An overnight culture of *E. coli* AB1157 was diluted 100-fold in NB, and then the cells were grown for 4 h at 30 °C under shaking. The number of cells in different variants of the experiment were equalized: the effects of AuHCl$_4$ on bacterial cells were compared by way of overnight culture diluted 10 times in NB (stationary phase) and a culture was grown in NB for 4 h (exponential phase). AuHCl$_4$ was added to both cultures and the solutions were shaken for 2 h. Then, the cells were plated on NA medium with 1.5% agar.

### 2.3.5. Statistical Analysis

The results related to MIC and biofilm characterizations were expressed in terms of the mean of *n* numbers of independent experiments standard deviation (SD). The data were analyzed using Microsoft Excel software.

## 3. Results and Discussions

### 3.1. Photocatalytic Bactericidal Effect and Femtosecond Laser Spectroscopy of Au/TiO$_2$ Suspensions

Figure 1 shows the CFU decay of *E. coli* AB1157 in aqueous solution photocatalyzed by suspensions of TiO$_2$ and Au/TiO$_2$ in the dark and also under visible light irradiation. Bacterial inactivation in the dark was not observed in Au/TiO$_2$ and TiO$_2$ suspensions. This indicates that Au/TiO$_2$ and TiO$_2$ are not intrinsically toxic towards *E. coli* AB1157. Moderate bacterial inactivation kinetics were induced by TiO$_2$, as shown in Figure 1 (trace 2), due to the TiO$_2$ surface states' excitation under visible light irradiation [31]. A higher acceleration in the *E. coli* AB1157 CFU bacterial inactivation kinetics is seen in Figure 1 (trace 1) for suspensions of Au/TiO$_2$ under visible light, as compared to TiO$_2$. Heating of Au-NPs was estimated to not exceed 1 °C (see Supplementary Information, Section SI4). Measurement of the temperature of the Au/TiO$_2$ suspension under visible light showed a heating of no more than 2 °C. Acceleration of the death of bacteria cannot be associated with the thermal effect. The insert in Figure 1 shows the absorption spectra of the Au/TiO$_2$ suspension. The absorption bands with maximum at ~550 nm of the Au/TiO$_2$ spectra correspond to the plasmon band of the Au-NPs in the nanocomposite (see insert A of Figure 1).
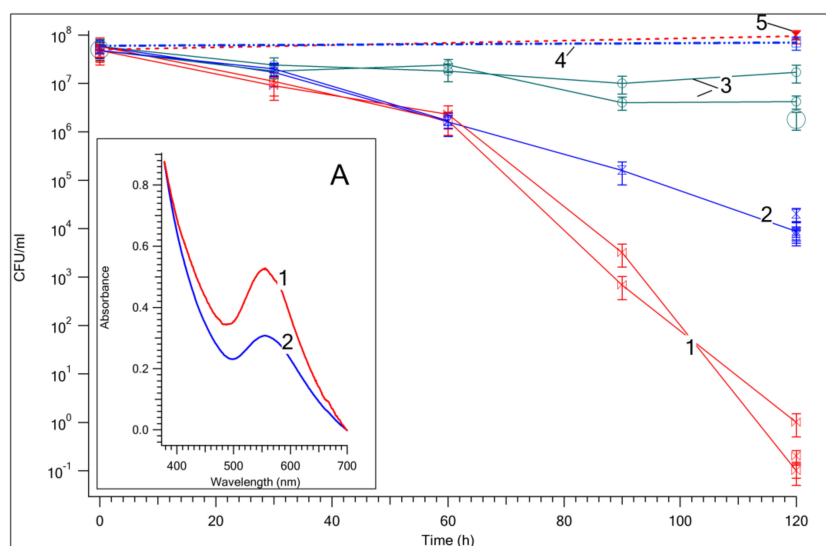


**Figure 1.** CFU/ml plotted as a function of *E. coli* AB 1157 inactivation time for solutions: 1, Au/TiO$_2$ suspension irradiated under visible light; 2, TiO$_2$ suspension irradiated under visible light; 3, water irradiated under visible light; 4, Au/TiO$_2$ suspension in dark; 5, TiO$_2$ suspension in dark. Insert A: spectrum 1, absorption spectrum of Au/TiO$_2$ before visible light irradiation; spectrum 2, absorption spectrum of Au/TiO$_2$ after 2 h under visible light in nutrient broth (NB).

Figure 2 demonstrates the transient absorption spectra of $Au/TiO_2$ suspension at a time delay shorter than 400 fs. The transient spectra consist of a bleaching band where a differential absorbance is negative $\Delta A < 0$ and an absorption band where a differential absorbance is positive $\Delta A > 0$. The bleach band position is close to maximum of the plasmon band. The appearance of the bleach band and the long wavelength absorption band is due to the shift and broadening of the plasmon resonance band in the photoexcited Au-NPs, due to the heating of the electron gas in the Au-NPs during the plasmon decay. This involves formation of a nonequilibrium electron and a subsequent thermalization process. The transient curve of the bleaching band amplitude shown in the insert of Figure 2 reveals the dynamics of the electron thermalization dynamics. Insert of Figure 2 shows the significant shift of the bleach band position that cannot be explained by the electron heating [19]. If the permittivity of the $TiO_2$ in the $Au/TiO_2$ NPs is changed, the position of the plasmon band is also shifted. Electrons injected from Au-NPs into $TiO_2$ lead to an increase in the $TiO_2$ refractive index ($n_{TiO2}$) and permittivity $\varepsilon_{TiO2} = (n_{TiO2})^2$ [19]. The change of permittivity can be a reason for the strong spectral shift of the plasmon band. Since the maximum position of the plasmon band is determined by the Fröhlich condition: $Re(\varepsilon_{Au}(\omega)) = -2\varepsilon_m$, the increase in the medium permittivity is due to the increase of $\varepsilon_{TiO2}$. This is associated with: (a) the long-wavelength shift of the plasmon band after Au-NP excitation and (b) the corresponding short-wavelength shift of the bleaching band seen in Figure 2. The dissolution of Au-NPs from the $Au/TiO_2$ surface occurs concomitantly with the transfer of electrons generated by Au plasmon into the conduction band of $TiO_2$. Under visible light, the Au-NP valence band holes ($v_bh^+$) give rise to Au ions that are released to the surrounding media. Electron injection from Au-NPs into $TiO_2$ agrees with a recent study by Tian and Tatsuma [32]. The antibacterial effects of these Au ions in solution will be addressed in detail in the sections below.
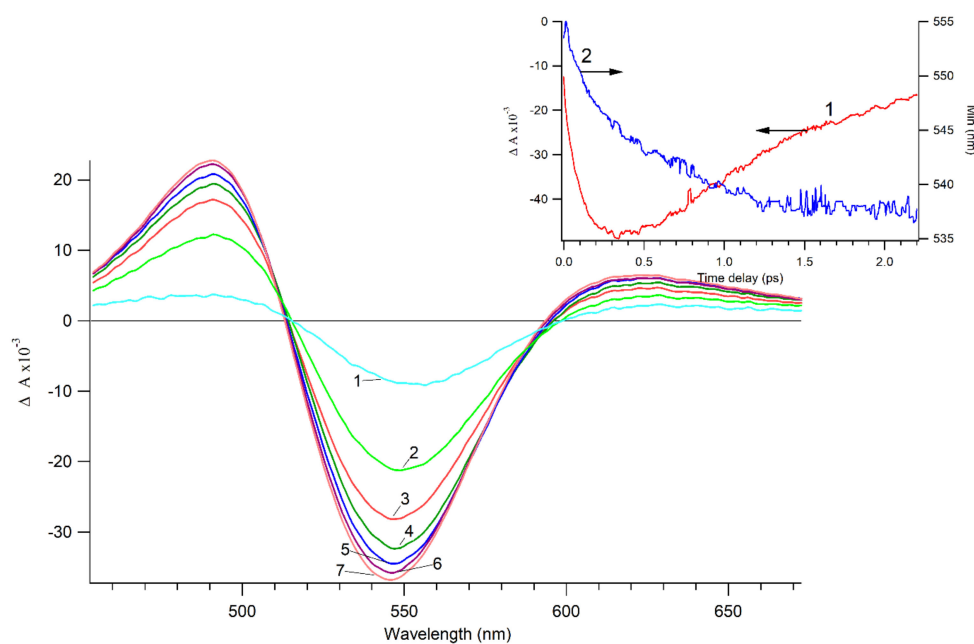


**Figure 2.** Transient absorption spectra $\Delta A$ ($\lambda$) of $Au/TiO_2$ suspension after excitation by a 25-fs laser pulse at 740 nm. Time delay: 1, 0 fs; 2, 50 fs; 3, 100 fs; 4, 150 fs; 5, 200 fs; 6, 250 fs; 7, 350 fs. Insert: Trace 1: the left y-axis shows the amplitude of the plasmon bleaching band; Trace 2: the right y-axis shows the wavelength of the minimum of the plasmon bleaching band.

Transmission electron microscopy images of $Au/TiO_2$ NPs before and after 24 h irradiation (see Figure 3) with LED green light (300 $\mu W/cm^2$) show that irradiation leads to the creation of chemical species associated with the fragmented Au-NPs. Bright- and dark-field transmission electron microscopy (TEM) images are shown in the Supplementary Information, Section SI5 (Figure SI4). This NPs fragmentation was not detected under similar visible light irradiation of pure $TiO_2$.

This observation agrees with the decrease of the plasmon band amplitude shown in the insert of Figure 1. Elemental analysis of Au/TiO$_2$ nanoparticles before and after 24 h irradiation shown the decrease of the Au in the Au/TiO$_2$ powder. This confirms the Au dissolution due to the surface plasmon resonance in the Au/TiO$_2$ bands.
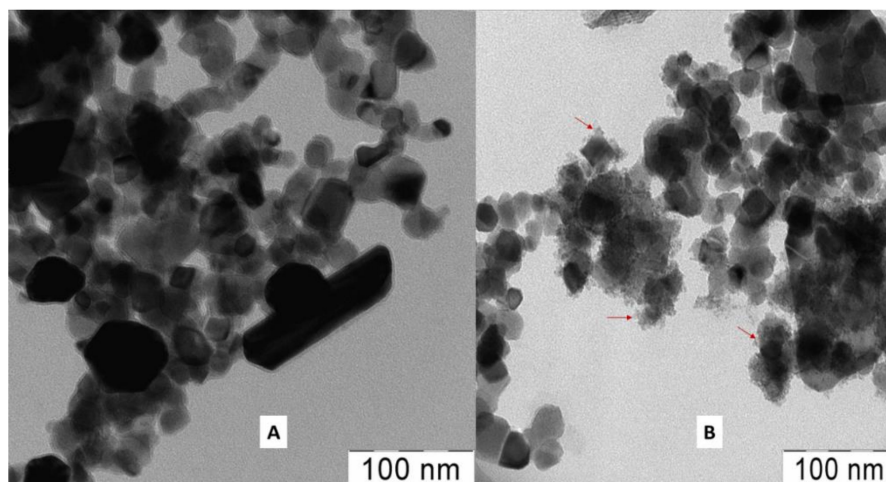


**Figure 3.** Images of Au/TiO$_2$ nanoparticles before and after 24 h irradiation with LED green light (300 µW/cm$^2$). (**A**) Au/TiO$_2$ nanoparticles before irradiation; (**B**) Au/TiO$_2$ nanoparticles after irradiation. Arrows indicate fine formations. LED: light-emitting diode.

*3.2. MICs of AuHCl$_4$ for Different Gram-Type Bacteria and Effect of AuHCl$_4$ on the Biofilm Formation*

3.2.1. MICs of AuHCl$_4$ of Different Gram-Type Bacteria

The bacteria cells for the determination of MICs were cultured in NB medium. The MIC values of AuHCl$_4$ measured for Gram-negative bacteria (*E. coli* AB1157, *P. aeruginosa* PAO1, and *S. proteamaculans* 94) are summarized in Table 1. The MIC values for *E. coli* AB1157 and *S. proteamaculans* 94 were close, and the resistance of *P. aeruginosa* PAO1 to AuHCl$_4$ was much higher. We examined effect of Au nanoparticles on *E. coli* AB1157 cells. Spherical Au nanoparticles and Au nanorods did not inactivate *E. coli* AB1157 cells. As some precursors of nanoparticles, such as the detergent CTAB, might induce toxicity, the nanoparticles themselves are not necessarily detrimental to cellular function (see Section SI6). This result agrees with conclusions made by Connor et al. [11].

3.2.2. Effect of AuHCl$_4$ on the Formation of Biofilms

Figure 4 shows the effect of AuHCl$_4$ on the planktonic growth (OD$_{600}$) and biofilm formation evaluated by the absorbance of crystal violet staining of biofilms of *E. coli* AB1157, *P. aeruginosa* PAO1, and *S. proteamaculans* 94. Planktonic growth was practically absent at a concentration of AuHCl$_4$ of 0.64 µg/mL for *E. coli* AB1157, 80 µg/mL for *P. aeruginosa* PAO1, and 5 µg/mL for *S. proteamaculans* 94. The decrease of the bacterial mass in the biofilm was detected by the A$_{600}$ absorbance. This was observed when the AuHCl$_4$ concentration was > 0.04 µg/mL for *E. coli* AB1157, 40 µg/mL for *P. aeruginosa* PAO1, and 2.5 µg/mL for *S. proteamaculans* 94. OD$_{600}$ of the biofilm biomass decreased almost to zero at AuHCl$_4$ concentrations of 0.64 µg/mL for *E. coli* AB1157, 10 µg/mL for *S. proteamaculans* 94, and >160 µg/mL for *P. aeruginosa* PAO1.
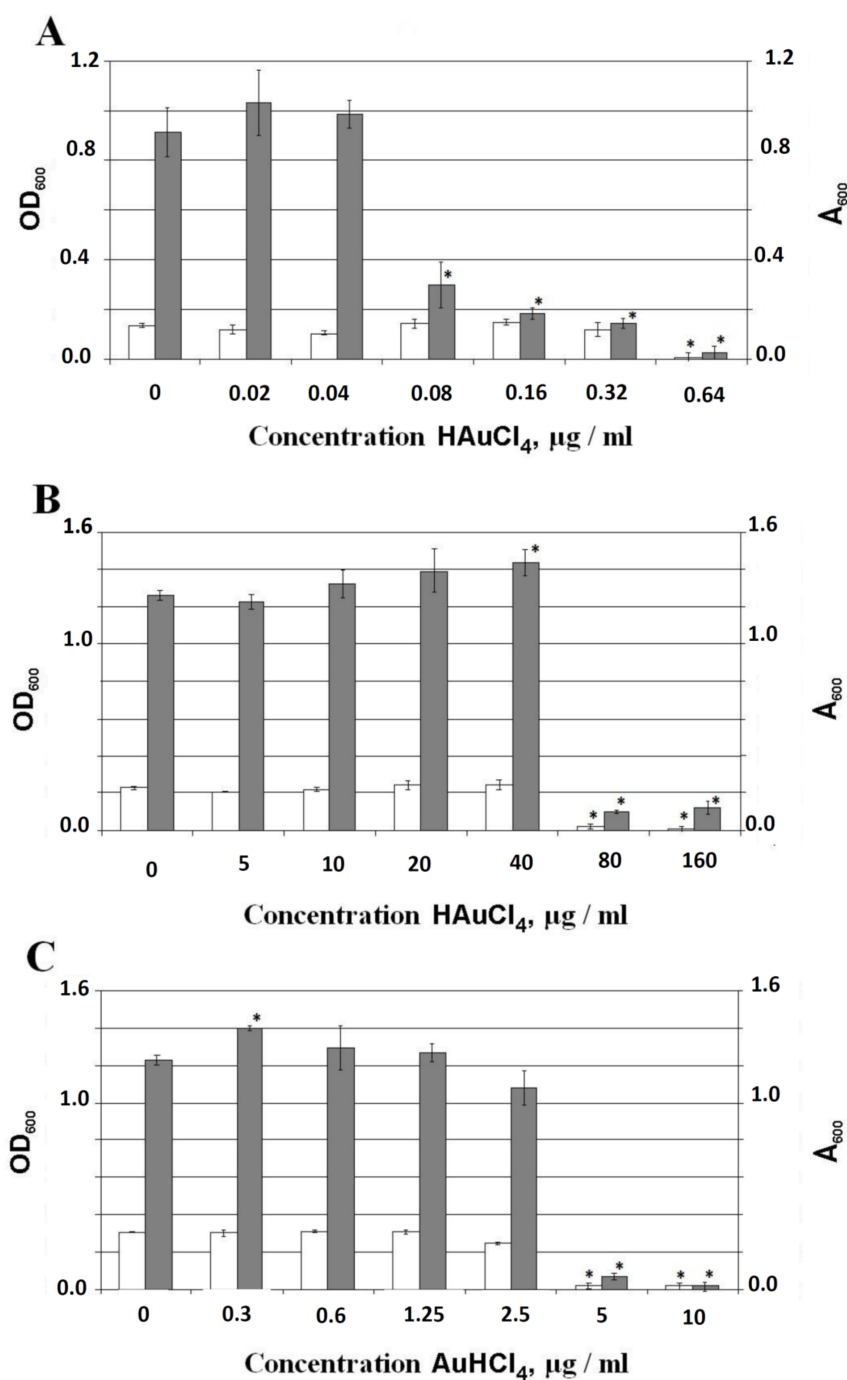
**Figure 4.** Effect of AuHCl$_4$ on biofilm formation and planktonic cells. (**A**) *E. coli* AB1157. (**B**) *P. aeruginosa* PAO1. (**C**) *S. proteamaculans* 94. OD$_{600}$, optical density of planktonic cells; A$_{600}$, absorption of crystal violet staining of biofilms. White bars refer to planktonic growth; dark bars refer to biofilms. Errors were determined from a set of 4 measurements with 8 replicate samples. The standard deviation is shown in the figures. According to the Student's *t*-test ($p < 0.05$), the bars marked with an asterisk (*) are significantly different from the negative (untreated) control (0 μg/mL of AuHCl$_4$). The mean CFU/ml for negative (untreated) controls were: ~1.8 × 10$^8$, 2.2·× 10$^8$, and 3.0·× 10$^8$ for *E. coli* AB1157, *P. aeruginosa* PAO1, and *S. proteamaculans* 94, respectively.

### 3.2.3. Effect of AuHCl$_4$ on Mature Biofilms of *E. coli* AB1157

The biofilms were grown in NB on glass slides under static conditions (without shaking). After biofilm growth for 24 h, the culture of planktonic cells was removed and a fresh NB solution

containing $AuHCl_4$ up to 150 µg/mL was added. Analysis of the biofilms with crystal violet staining showed that the decrease in the biofilms began at an $AuHCl_4$ concentration of 3–15 µg/mL. An increase in the $AuHCl_4$ concentration led to a further decrease of the biofilm biomass (Figure 5). Figure 6 presents the confocal microscopy images of *E. coli* AB1157 biofilms without $AuHCl_4$ treatment (a, control, green cells) and after the treatment by 15 µg/mL (b) and 150 µg/mL (c) $AuHCl_4$. The treatment of biofilms with 150 µg/mL of $AuHCl_4$ led to cell death in the biofilms (red cells). This shows that the $AuHCl_4$ concentrations completely inhibiting biofilm formation of *E. coli* were insufficient to kill bacterial cells in mature biofilms. The existence of bacteria in biofilms protected them from the action of $AuHCl_4$. Figure 6 shows that *E. coli* cells died at an $AuHCl_4$ concentration of 150 µg/mL. However, at a similar $AuHCl_4$ concentration, the biofilm biomass decreased by only ~1.6 times from $A_{600}$ 0.8 to 0.5 (see Figure 5). This shows that the matrix biofilm mass was less reduced compared to the living cells in the biofilm.
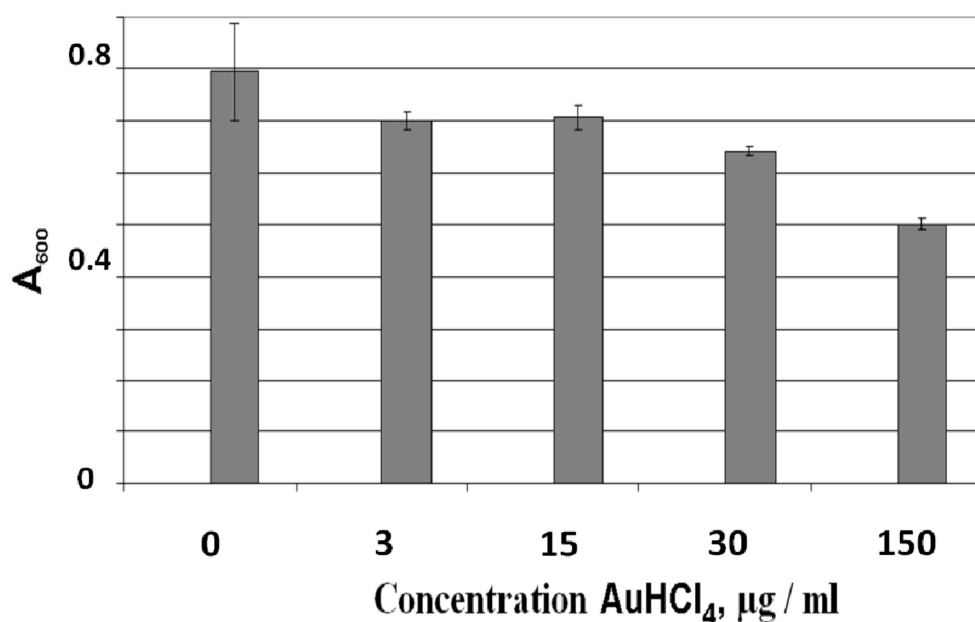


**Figure 5.** Effect of $AuHCl_4$ concentration on the mature biofilms. $A_{600}$ is the absorption of crystal violet-stained biofilms, which is a measure of the biofilm biomass. Errors were determined from a set of 4 measurements with 8 replicate samples.
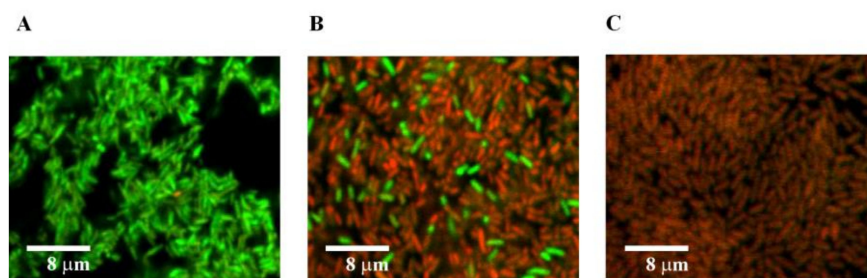


**Figure 6.** Confocal microscopy of *E. coli* AB1157 biofilms. (**A**) Confocal microscopy of *E. coli* AB1157 cells at 0 µg/mL $AuHCl_4$; (**B**) at 15 µg/mL; (**C**) at 150 µg/mL $AuHCl_4$. Viable cells are shown by green color and dead cells by red.

### 3.3. The Effect of Phase of Growth on the Sensitivity of E. coli AB1157 Cells to AuHCl_4

To clarify the increased resistance of bacterial biofilms to the action of Au ions, the survival of *E. coli* cells in the presence of $AuHCl_4$ was investigated at different growth stages. The high density of bacteria in biofilms, the lack of access to nutrients and oxygen, and metabolite accumulation of the bacteria inside the biofilms are similar to those in the physiological state with the cells in a stationary

phase or in a phase of growth retardation. Since the bacterial cells in a stationary growth phase are usually more resistant to unfavorable external effects, it is assumed that the physiological state of cells living in biofilms led to the cells' high resistance. The influence of the growth phase on the sensitivity of bacteria to Au compounds has not been reported. We showed that resistance to the action of AuHCl$_4$ of *E. coli* AB1157 cells in the early stationary phase of growth was higher than that in the exponential-phase cells (see Table 2).

**Table 2.** The influence of phase of growth on survival of *E. coli* AB1157 in solutions with Au ions*.

| AuHCl$_4$ (µg/mL) | Exponential Phase of Growth (cells/mL) | | Stationary Phase of Growth (cells/mL) | |
|---|---|---|---|---|
| 0 | $16 \cdot \times 10^7$ | 100% ** | $22 \cdot \times 10^7$ | 100% |
| 5 | $1.4 \cdot \times 10^7$ | 8.8% | $8.2 \cdot \times 10^7$ | 38% |
| 8.5 | $8 \times 10^5$ | 0.5% | $12.6 \cdot \times 10^6$ | 6% |
| 17 | $4.8 \cdot \times 10^5$ | 0.3% | $5 \cdot \times 10^6$ | 2.3% |

* Data from triplicate runs. ** Percentage of colonies in the control (without AuHCl$_4$).

### 3.4. About the Effect of the Au Ions' Interaction with Bacteria

Earlier work on the mechanisms of silver ions' and silver nanoparticles' interaction with bacterial cells [26] demonstrated that the increased cell sensitivity to the silver ions/NPs was due to mutations in the genes responsible for DNA repair of the oxidative damage (*mut*Y, *mut*S, *mut*M, *mut*T, *nth*). We have assumed on the basis of this data that these genes are involved in the restoration of DNA oxidatively damaged by silver compounds. Because cellular DNA could be damaged by AuHCl$_4$, it was interesting to determine if the DNA repair is involved in the protection of cells from Au ions. For this purpose, we compared the AuHCl$_4$ MICs for isogenic *E. coli* wild-type strains and mutant strains deficient in different repair systems. The data is presented in Table 3. There is no information at the present time in the available literature regarding the participation of DNA repair systems in the protection of bacterial cells toward Au ions. Upon comparison of the sensitivity to Au ions of cells of *E. coli* BW25113 (wild-type strain) and a number of mutants deficient in proteins involved in oxidative DNA repair (*mut*Y, *mut*S, *mut*M, *mut*T, *nth*), no significant differences were found between these strains (see Table 3). The slight increase in sensitivity to the Au ions was observed in the bacterial cells with the mutations in the *mut*S and *mut*Y genes. Enzymes encoded by these genes remove adenine bases that are misincorporated opposite to 8-oxoG (8-oxoguanine, the most common oxidative lesion) [33–35]. The data shows that the sensitivity of cells to Au ions is not significantly related to oxidative DNA damage by Au ions. Mutant strains deficient in SOS repair genes (*rec*A, *lex*A, *umu*C, *umu*D) showed practically the same sensitivity to AuHCl$_4$ as the wild-type strains (see Table 3). This means that the genes involved in DNA repair are not important for the bacteria cell resistance to AuHCl$_4$. Mutation in the *uvr*A6 gene did not increase significantly the sensitivity of *E. coli* to Au ions. It is known that the global regulator sigma S subunit of RNA polymerase encoded by *rpoS* controls the transcription of a large number of genes under various types of stress. Genes activated by sigma S encode proteins that protect cells from stress [36]. It is expected that cells harboring the *rpoS* mutation would be more sensitive to the action of AuHCl$_4$. However, the sensitivity to Au ions of cells presenting this mutation was almost unchanged. Porins are the proteins of the outer membrane in Gram-negative bacteria present in the water-filled channels enabling the influx and efflux of low-molecular-weight compounds through the outer membrane of the bacterial cell [37]. *E. coli* mutants deficient in OmpF and/or OmpC porins were 4–8 times more resistant to Ag ions. This validates their important role in the transport of silver ions to the bacterial cell [26,38,39]. Mutant strains lacking porins OmpF or OmpC did not differ significantly in their sensitivity to Au ions as compared to the wild-type strain. The mechanism of bactericidal action of Au ions and Ag ions on bacterial cells are substantially different.

**Table 3.** AuHCl$_4$ MICs of *E. coli* strains with deficiency in DNA repair, in global regulation of genes expression, and in porin synthesis.

| Strains of *Escherichia coli* K12 | Characteristics | MIC of AuHCl$_4$, µg/mL* |
|---|---|---|
| SBS 1936 | *rpo* S$^+$ | $1.3 \pm 0.2$ |
| SBS 2680 | *rpo* S$^-$ | $1.0 \pm 0.3$ |
| AB 1157 | *uvr*A$^+$ *uvr*B$^+$ *rec*A$^+$ *lex*A$^+$ *rec*BC$^+$ *rec*F$^+$ *lon*$^+$ | $1.0 \pm 0.3$ |
| AB 1886 | *uvr* A6 | $0.5 \pm 0.2$ |
| AB 2463 | *rec* A13 | $0.7 \pm 0.2$ |
| AB 2494 | *lex* A | $1.0 \pm 0.3$ |
| MC 4100 | *omp*R$^+$ *omp*F$^+$ *omp*C$^+$ | $1.0 \pm 0.3$ |
| TK 821 | *omp*R$^+$ *omp*F$^-$ *omp*C$^-$ | $1.3 \pm 0.3$ |
| MH 1471 | *omp*R$^+$*omp*F$^-$ *omp*C$^+$ | $1.0 \pm 0.3$ |
| MH 225 | *omp*R$^+$*omp*F$^+$ *omp*C$^-$ | $1.0 \pm 0.3$ |
| BW 25113 | | $1.0 \pm 0.3$ |
| JW 2703 | *rrn*B3 Δ*lac*Z4787 *hsd*R514 | $0.5 \pm 0.2$ |
| JW 2928 | Δ(*araBAD*)567Δ(*rhaBAD*)568 *rph-1* | $0.5 \pm 0.2$ |
| JW 3610 | *mutS::kanmutY::kanmutM::kanmutT::kan* | $1.3 \pm 0.3$ |
| JW 0097 | | $1.0 \pm 0.3$ |
| TK 603 | | $1.0 \pm 0.3$ |
| TK 610 | *uvr* A6*umu* C36*umu* C44 | $1.0 \pm 0.3$ |
| TK 612 | | $0.8 \pm 0.2$ |

* Values of MICs are obtained from data from 5 independent runs.

### 3.5. The Effect of the Au Ions' Interaction with Bacteria

Only a few reports have addressed the effect of Au ions on bacterial cells [22]. As noted in the preceding sections in this study, cells in mature biofilms are more resistant to drugs/antibiotics and unfavorable environmental factors when exposed to their effects than planktonic cells. Only a few reports are available reporting data on the resistance of biofilms to silver ions and silver NPs, or on the effect of the later compounds on the growth/biofilm formation by planktonic cells. During the course of this work, we did not find data about the effect of Au ions on the formation of biofilms and mature biofilms in the literature. This motivated us to investigate this problem. The mechanism of the high resistance of bacteria observed in biofilms is extremely important in the field of antibiotic therapy.

During this work, we found that Au ions inhibit biofilm formation and cause cell death on preformed biofilms. The cell death in mature biofilms was observed at higher concentrations of Au ions compared to the Au concentration required during the film formation stage. Bacteria in biofilms were up to 150 times more resistant to the action of AuHCl$_4$ than planktonic cells. The increased resistance of bacterial cells in biofilms has been reported for the salts of copper, lead, zinc [40], silver ions, and silver nanoparticles [26,41]. The biofilm resistance has been reported to depend on the penetration of antimicrobial agents in the biofilm matrix, the metabolic activity and growth rate of biofilm bacteria and planktonic growing cells, and on the population of persistent cells able to survive stress conditions [41,42]. The physiological condition and the metabolic activity of cells living in biofilms are closer to those in the stationary phase than the cells in the growth stage. This is one reason for the increased cell resistance to unfavorable factors. It is known that bacteria in the growth phase of growth retardation and in the stationary phase are more resistant to antibacterial agents. This is important in relation to antibiotics targeting cell division. One study reported that the increased resistance of bacteria in biofilms involves a multifactorial process [43].

The resistance of bacteria cells to Au ions within the growth phase has not been reported. The present study shows that that the *E. coli* cells in the growth phase were significantly more resistant to Au ions than cells in the logarithmic phase. Thus, it can be assumed that the increased cell resistance in biofilms to AuHCl$_4$ is due to the physiological state of the bacteria inside the biofilm being similar to the state of the cells in the stationary growth phase. We did not obtain data about participation of DNA repair systems in the protection of the bacterial cells against Au ions. There were no significant differences in the sensitivity of bacteria to Au ions in comparison with wild-type strains and mutant

strains deficient in SOS repair (*rec*A, *lex*A, *umu*C, *umu*D), excision repair (*uvr*6) or DNA repair of oxidative damage caused by ROS (reactive oxygen species) (*mut* S, *mut*Y, *mut*M, *mut*T). These data suggest that the sensitivity of bacteria to Au ions is not related to DNA damage that can be recovered by way of DNA repair systems. It can be assumed that the effect of Au ions on the bacterial cells is mainly due to the binding of Au ions to the DNA bases. This interaction has been reported to be important in the case of silver ions and preferably occurs with GC pairs of the DNA, leading to serious damage [44,45]. However, detailed study of DNA damage due to Au ions was not carried out during the course of this study. Cell mechanisms that may be involved in the repair of cell damage is also lacking at the present time.

It has been shown that mutant strains with inactivated genes encoding the transport proteins porins did not differ significantly in their sensitivity to Au ions compared to the wild-type strain. Thus, it can be concluded that porins are not involved or only partially involved in the transport of Au ions in the cells. This is not the case for the transport of silver ions [26]. This observation suggests the possibility of other mechanisms taking place during the Au ion penetration into the cells. The removal of metal by means of active transport through transporter proteins from the cytoplasm to the periplasmic space is well-known to be involved with bacterial resistance to metals [43]. Binding of Au ions on the cell membrane is also possible, similar to the adsorption of other heavy metal ions [46].

### 3.6. Benefits of the Information Reported in This Study: Outlook and Future Work

Healthcare-associated infections (HCAIs) present a major public health problem worldwide. Hospitals are a reservoir of pathogenic microorganisms, leading to a higher incidence of HCAIs. During the last few years, an increase in HCAIs caused by mutant pathogen strains, especially drug-resistant strains, has been noticed in hospitals. Occurrence of infections resistant to both the immune system and antibiotics has increased during the last decade. Vancomycin and gentamicin are used in combating infections caused by biofilms on tissues and implants, but their action does not exceed a few days and is irregular.

Biofilms are the most dangerous type of bacterial presence, spreading infections over long time periods, and this is the reason why some aspects of the $Au/TiO_2$ interaction with biofilms have been documented in a quantitative way and presented in detail in this study. More advanced antimicrobial materials at this stage are necessary, and $Au/TiO_2$ releasing low-cytotoxicity Au ions is shown to present antimicrobial activity with advantages compared to antibiotics. The later compounds promote the development of bacterial resistance when administered over longer treatment periods. This study has shown that $Au/TiO_2$ NPs disinfect bacteria by releasing adequate amounts of Au ions while keeping sufficient reserves to ensure long-term operational disinfection. Metals can eliminate/destroy more than 99% of the microbial strains, and antibiotics coupled with Au ions are not available at the present time. They could improve the present situation due to the small size of the Au ions enabling them to penetrate tissues not reached adequately by antibiotics. This study shows that Au ions in ppb concentrations lead to effective disinfection. This information may be used to assess if the concentrations of Au- ions leading to bacterial disinfection are below the guidelines imposed by sanitary regulations. This study presents basic information that can be useful for the preparation of Au-NPs on other substrates than $TiO_2$ to increase selectivity, giving high-quality functionalized Au coatings that reduce the toxicity to mammalian cells, while maintaining antimicrobial activity and a high biocompatibility. The development of $Au/TiO_2$ NPs activated by solar/visible/actinic light is in its infancy.

The bacterial cell membrane is both a barrier and a channel for the inward and outward movement of chemical species with sizes below the porin diameters. In the Gram-negative bacterial membrane structure, porins allow the passage of molecules <600 Da in and out of the bacteria. The small size of the metal ions allows the Au ions to enter the pathogen and translocate through the bacterial cell wall. However, we do not know the fate of the intracellular $Au/TiO_2$ NPs or Au ions. This is still a controversial issue and cannot be yet answered. The problem is that the majority of cell culture

studies are done under suspension, and thus then difficult to differentiate between the particle and ionic effects.

This study presents the interfacial interaction between $Au/TiO_2$ and bacteria in detail and suggests the mechanism leading to bacterial inactivation. However, the full bactericidal inactivation mechanism is still not understood. The $Au/TiO_2$ NPs exhibit promising antibacterial kinetics and offer a potential new approach for the effective prevention of bacterial infections by pathogenic biofilms, as investigated during the course of this study. The benefit of establishing the Au disinfection mechanism is that this is a necessary step for any commercial application of a light-induced antibacterial process.

## 4. Conclusions

This work presents femtosecond dynamics of $Au/TiO_2$ SPR plasmon-band decay leading concomitantly to the generation of toxic Au ions that subsequently induce bacterial inactivation in different bacterial strains. The effects $AuHCl_4$ on the cell biofilm formation and planktonic cells is reported in a quantitative way. This study reports some aspects related to the effect of mutations in the genes responsible for DNA repair and on the sensitivity of *E. coli* to the Au ions in a detailed way. Au ions were found to inhibit biofilm formation and led to cell death in preformed biofilms. To achieve cell death in mature biofilms required higher Au ion concentrations compared to the Au concentrations needed for the biofilms investigated during the early formation stages.

This study also reports on the Au ions' mechanism of interacting with the bacterial cells. This has not previously reported and was found to be different compared to the interaction with Ag ions. This study also reports on the effect of gene mutations responsible for DNA repair and on the sensitivity of *E. coli* to the Au ions.

## References

1. Jalvo, B.; Faraldos, M. Antimicrobial and antibiofilm efficacy of self-cleaning surfaces functionalized by $TiO_2$ photocatalytic nanoparticles against *Staphylococcus aureus* and *Pseudomonas putida*. *J. Hazard. Mater.* **2017**, *340*, 160–170. [CrossRef] [PubMed]

2. Yadav, H.M.; Kim, J.S. Developments in photocatalytic antibacterial activity of nano $TiO_2$: A review. *Korean J. Chem. Eng.* **2016**, *33*, 1989–1998. [CrossRef]

3. Fagan, R.; McCormack, D.E. A review of solar and visible light active $TiO_2$ photocatalysis for treating bacteria, cyanotoxins and contaminants of emerging concern. *Semicond. Process.* **2016**, *42*, 2–14. [CrossRef]

4. Wilke, C.M.; Gaillard, J.F. The critical role of light in moderating microbial stress due to mixtures of engineered nanomaterials. *Environ. Sci. Nano* **2018**, *5*, 96–102. [CrossRef]

5. Armelao, L.; Barreca, D. Photocatalytic and antibacterial activity of $TiO_2$ and $Au/TiO_2$ nano-systems. *Nanotechnology* **2007**, *18*, 375709. [CrossRef]

6. Pan, Y.; Leifert, A. Gold nanoparticles of diameter 1.4 nm trigger necrosis by oxidative stress and mitochondrial damage. *Small* **2009**, *5*, 2067–2076. [CrossRef] [PubMed]

7. Wang, S.; Lawson, R. Toxic effects of gold nanoparticles on Salmonella typhimurium bacteria. *Toxicol. Health* **2011**, *27*, 547–554. [CrossRef] [PubMed]

8.　Zhou, Y.; Kong, Y. Antibacterial activities of gold and silver nanoparticles against *Escherichia coli* and bacillus Calmette-Guérin. *J. Nanobiotechnol.* **2012**, *10*, 19. [CrossRef]

9.　Cui, Y.; Zhao, Y. The molecular mechanism of action of bactericidal gold nanoparticles on *Escherichia coli*. *Biomaterials* **2012**, *33*, 2327–2333. [CrossRef]

10.　Bresee, J.; Maier, K.E. Growth inhibition of *Staphylococcus aureus* by mixed monolayer gold nanoparticles. *Small* **2011**, *7*, 2027–2031. [CrossRef] [PubMed]

11.　Connor, E.E.; Mwamuka, J. Gold nanoparticles are taken up by human cells but do not cause acute cytotoxicity. *Small* **2005**, *1*, 325–327. [CrossRef] [PubMed]

12.　Rahme, K.; Chen, L. PEGylated gold nanoparticles: Polymer quantification as a function of PEG lengths and nanoparticle dimensions. *RSC Adv.* **2013**, *3*, 6085–6094. [CrossRef]

13.　Zhang, W.; Li, Y. Photogeneration of reactive oxygen species on uncoated silver, gold, nickel, and silicon nanoparticles and their antibacterial effects. *Langmuir* **2013**, *29*, 4647–4651. [CrossRef] [PubMed]

14.　Silvero, M.J.; Becerra, M.C. Plasmon-induced oxidative stress and macromolecular damage in pathogenic bacteria. *RSC Adv.* **2016**, *6*, 100203–100208. [CrossRef]

15.　Zharov, V.P.; Mercer, K.E. Photo-termal nano-therapeutics and nano-diagnostics for selective killing of bacteria targeted with gold nanoparticles. *Biophys. J.* **2006**, *90*, 619–627. [CrossRef] [PubMed]

16.　Calixto, G.M.; Bernegossi, J.J. Nanotechnology-Based Drug Delivery Systems for Photodynamic Therapy of Cancer: A Review. *Molecules* **2016**, *21*, E342. [CrossRef] [PubMed]

17.　Ngwa, W.; Kumar, R. Targeted radiotherapy with gold nanoparticles: Current status and future perspectives. *Nanomed. (Lond.)* **2014**, *9*, 1063–1082. [CrossRef]

18.　Her, S.; Jaffray, D.A. Gold nanoparticles for applications in cancer radiotherapy: Mechanisms and recent advancements. *Adv. Drug Deliv. Rev.* **2015**, *S0169-409X*, 30014. [CrossRef]

19.　Aiboushev, A.; Gostev, F. Spectral properties of the surface plasmon resonance and electron injection from gold nanoparticles to $TiO_2$ mesoporous film: Femtosecond study. *Photochem. Photobiol. Sci.* **2013**, *12*, 631–637. [CrossRef]

20.　Cushing, S.K.; Chen, C.J. Tunable Nonthermal Distribution of Hot Electrons in a Semiconductor Injected from a Plasmonic Gold Nanostructure. *ACS Nano* **2018**, *12*, 7117–7126. [CrossRef]

21.　Nies, D.H. Microbial heavy-metal resistance. *Appl. Microbiol. Biotechnol.* **1999**, *51*, 730–750. [CrossRef] [PubMed]

22.　Checa, S.K.; Soncini, F.C. Bacterial gold sensing and resistance. *Biometals* **2011**, *24*, 419–427. [CrossRef] [PubMed]

23.　Benedek, T.G. The history of gold therapy for tuberculosis. *J. Hist. Med. Allied Sci.* **2004**, *59*, 50–89. [CrossRef] [PubMed]

24.　Milacic, V.; Fregona, D. Gold complexes as prospective metal-based anticancer drugs. *Histol. Histopathol.* **2008**, *23*, 101–108. [CrossRef] [PubMed]

25.　Shaw, C.F., III. Gold-Based Therapeutic Agents. *Chem. Rev.* **1999**, *99*, 2589–2600. [CrossRef]

26.　Radzig, M.A.; Nadtochenko, V.A. Antibacterial effects of silver nanoparticles on Gram-negative bacteria: Influence on the growth and biofilms formation, mechanisms of action. *Colloids Surf. B Biointerfaces* **2013**, *102*, 300–306. [CrossRef] [PubMed]

27.　Sau, T.K.; Murphy, C.J. Seeded high yield synthesis of short Au nanorods in aqueous solution. *Langmuir* **2004**, *20*, 6414–6420. [CrossRef]

28.　Turkevich, J.; Stevenson, P.C. A study of the nucleation and growth processes in the synthesis of colloidal gold. *Discuss. Faraday Soc.* **1951**, *11*, 55–75. [CrossRef]

29.　Nadtochenko, V.; Denisov, N. Ultrafast Spectroscopy of Fano-Like Resonance between Optical Phonon and Excitons in CdSe Quantum Dots: Dependence of Coherent Vibrational Wave-Packet Dynamics on Pump Fluence. *Nanomaterials* **2017**, *7*, 371. [CrossRef]

30.　Zaitseva, J.; Granik, V. Effect of nitrofurans and generators on biofilm formation by *Pseudomonas aeruginosa PAO1* and *Burkholderia Cenocepacia 370*. *Res. Microbiol.* **2009**, *160*, 353–357. [CrossRef]

31.　Fujishima, A.; Zhang, X. $TiO_2$ photocatalysis and related surface phenomena. *Surf. Sci. Rep.* **2008**, *63*, 515–582. [CrossRef]

32.　Tian, Y.; Tatsuma, T. Mechanisms and applications of plasmon-induced charge separation at $TiO_2$ films loaded with gold nanoparticles. *J. Am. Chem. Soc.* **2005**, *127*, 7632–7637. [CrossRef] [PubMed]

33. Matsumoto, Y.; Zhang, Q.M. *Escherichia coli* Nth and human hNTH1 DNA glycosylases are involved in removal of 8-oxoguanine from 8-oxoguanine/guanine mispairs in DNA. *Nucleic Acids Res.* **2001**, *29*, 1975–1981. [CrossRef] [PubMed]

34. Wyrzykowski, J.; Volkert, M.R. The *Escherichia coli* methyl-directed mismatch repair system repairs base pairs containing oxidative lesions. *J. Bacteriol.* **2003**, *185*, 1701–1704. [CrossRef] [PubMed]

35. David, S.S.; O'Shea, V.L. Base-excision repair of oxidative DNA damage. *Nature* **2007**, *447*, 941–950. [CrossRef] [PubMed]

36. Hengge-Aronis, R. Signal transduction and regulatory mechanisms involved in control of the σ$^S$(rpoS) subunit of RNA Polymerase. *Microbiol. Molec. Biol. Revs.* **2002**, *66*, 373–395. [CrossRef]

37. Nikaido, H. Porins and specific diffusion channels in bacterial outer membranes. *J. Biol. Chem.* **1994**, *269*, 3905–3908.

38. Pugsley, A.P.; Schnaitman, C.A. Outer membrane proteins of *Escherichia coli*. VII. Evidence that bacteriophage-directed protein 2 functions as a pore. *J. Bacteriol.* **1978**, *133*, 1181–1189.

39. Li, X.Z.; Nikaido, H. Silver-resistant mutants of *Escherichia coli* display active efflux of Ag+ and are deficient in porins. *J. Bacteriol.* **1997**, *179*, 6127–6132. [CrossRef]

40. Teitzel, G.M.; Parsek, M.R. Heavy metal resistance of biofilm and planktonic Pseudomonas aeruginosa. *Appl. Environ. Microbiol.* **2003**, *69*, 2313–2320. [CrossRef]

41. Bjarnsholt, T.; Kirketerp-Moller, K. Silver against Pseudomonas aeruginosa biofilms. *APMIS* **2007**, *115*, 921–928. [CrossRef] [PubMed]

42. Keren, I.; Shah, D. Specialized persistent cells and the mechanism of multidrug tolerance in *Escherichia coli*. *J. Bacteriol.* **2004**, *186*, 8172–8180. [CrossRef] [PubMed]

43. Summers, A.O. Damage control: Regulating defenses against toxic metals and metalloids. *Curr. Opin. Microbiol.* **2009**, *12*, 138–144. [CrossRef] [PubMed]

44. Calamai, P.; Carotti, S. Biological properties of two gold(III) complexes: AuCl$_3$(Hpm) and AuCl$_2$(pm). *J. Inorg. Biochem.* **1997**, *66*, 103–109. [CrossRef]

45. Marino, T.; Russo, N. Theoretical investigation on DNA/RNA base pairs mediated by copper, silver, and gold cations. *Dalton Trans.* **2012**, *41*, 1816–1823. [CrossRef] [PubMed]

46. Volesky, B.; Holan, Z.R. Biosorption of heavy metals. *Biotechnol. Progress* **1995**, *11*, 235–250. [CrossRef] [PubMed]